THE JOURNAL OF PHYSICAL CHEMISTRY C
A JOURNAL OF THE AMERICAN CHEMICAL SOCIETY

pubs.acs.org/JPCC

Article

Adsorption of Cyclic (Alkyl) (Amino) Carbenes on Monohydride Si(001) Surfaces: Interface Bonding and Electronic Properties

Lukas Meier and Wolf Gero Schmidt*

Cite This: *J. Phys. Chem. C* 2023, 127, 1973−1980

Read Online

ACCESS | Metrics & More | Article Recommendations

ABSTRACT: The adsorption of cyclic (alkyl) (amino) carbenes on the monohydride Si(001) surface is explored within density-functional theory. Two different adsorption mechanisms are investigated: the carbene insertion in Si−H bonds and the binding to a surface defect with missing hydrogen. The relative stability of these configurations depends on the hydrogen chemical potential, i.e., the surface preparation conditions as well as on the molecular side groups. The latter are also found to decisively influence the molecular diffusion. Some adsorption configurations are found to give rise to electronic states within the silicon bulk band gap. A sizable reduction of the work function is found upon molecular adsorption.

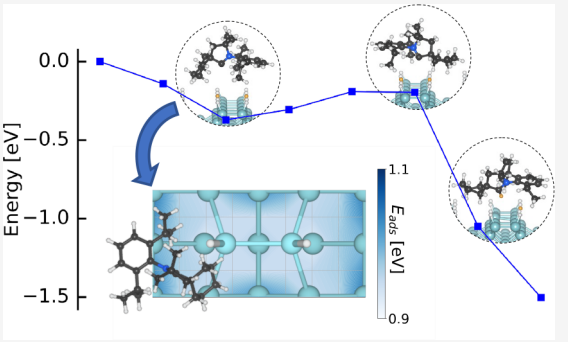

INTRODUCTION

There has been a long-standing interest in the functionalization of silicon surfaces.[1] While the ubiquitous oxide overlayer frequently utilized in silicon-based integrated circuits functions well for many microelectronic applications, there is an increasing desire to tailor the silicon surface and interface properties more specifically.[2] Organic surface functionalization allows for the synthesis of new classes of hybrid materials with the objective of combining the Si bulk electronic properties with tailored surface characteristics, such as tunable reactivity, biocompatibility, and hydrophobicity. Solar cells that pair the electron-selective contact of a high-efficiency silicon heterojunction with an organic singlet fission material are an intriguing example in this respect.[3,4] The properties of the organic−inorganic interfaces largely determine the functionality of the hybrid material, e.g., in terms of the solar cell efficiency.[5] In many instances, a work function reduction of surfaces is required in order to facilitate charge carrier transport. In this respect, surface modifiers that contain amine groups have proven very successful.[6]

N-Heterocyclic carbenes (NHCs) are cyclic compounds containing a divalent carbon atom bound to at least one nitrogen atom within the heterocycle.[9,10] They have proven to be excellent ligands that allow for the formation of highly ordered monolayers on metal surfaces, e.g., refs 11−18. The self-assembled monolayers based on NHCs show a remarkable resistance to heat and chemical reagents.[19] However, NHC adsorption on silicon has only rarely been studied.[8,20,21] Among NHCs, cyclic (alkyl) (amino) carbenes (CAACs) represent a prominent class of monoaminocarbenes, which exhibit particularly strong σ-donating properties.[22] Like all carbenes, these molecules possess two unpaired electrons at the carbene C atom leading to a high reactivity. Additionally, the atoms adjacent to the carbene C are an amino substituent and an sp^3-hybridized alkyl C atom, leading to a higher electrophilicity and nucleophilicity than for NHCs.[23] CAACs have been demonstrated to form short-range-ordered overlayers on coin metal surfaces.[24] While the general suitability of diamino NHCs to functionalize Si(111) has already been demonstrated,[21] there has been only one study on the adsorption of monoamino CAACs on Si surfaces: Zhukhovitskiy et al. investigated the adsorption of cyclohexyl CAAC (CyCAAC) on Si(111):H and proposed its suitability to functionalize Si(001):H.[8]

The present study computationally explores the adsorption of three different CAAC molecules, including CyCAAC, on the monohydride Si(001):H surface (Figure 1). Particular attention is paid to the bonding schemes, the surface diffusion properties, and the modification of the Si surface electronic properties in terms of interface states within the Si band gap and work function changes.

METHODOLOGY

The present study is based on the Vienna *ab initio* simulation package (VASP)[25] implementation of density-functional

Received: October 18, 2022
Revised: January 3, 2023
Published: January 19, 2023

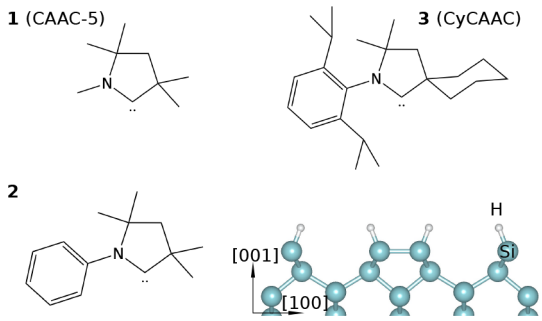

Figure 1. Molecules (**1** (CAAC-5[7]), **2**, and **3** (CyCAAC[8])) and the monohydride Si(001):H surface studied here.

theory (DFT). The generalized gradient approximation (GGA) is used to model the electron exchange and correlation interaction. In particular, we used the Perdew–Becke–Ernzerhoff (PBE) functional.[26] In order to account for the van der Waals interaction, dispersion-corrected DFT (DFT-D) is used.[27,28] Specifically, Grimme's D3 scheme with Becke–Johnson damping was applied.[29,30] The electron–ion interaction is described by projector-augmented waves (PAW).[31,32] The electronic wave functions are expanded into plane waves up to a kinetic energy of 450 eV. A force threshold of 0.01 eV/Å is used for the structural relaxations. The Si surface is simulated within a 4 × 4 periodic unit cell and a slab thickness of eight atomic layers. It is saturated with one hydrogen per Si surface atom, corresponding to the 2 × 1 dimerized monohydride phase[33] (Figure 1). The bottom three layers are frozen at the ideal bulk coordinates with a dihydrogen termination of the bottommost layer. A vacuum layer of 3 nm is used to decouple the slabs along the surface normal. Dipole corrections are applied for work function calculations. The surface Brillouin zone is sampled using a 2 × 2 × 1 Monkhorst–Pack mesh.[34] The mesh density is increased to 8 × 8 × 1 for density of states (DOS) calculations. In this case, a tetrahedral smearing with Blchl corrections[35] is used.

The molecular adsorption energies E_{ads} are calculated as

$$E_{ads} = E_{tot} - E_s - E_m \quad (1)$$

where E_{tot}, E_s, and E_m are the energies of the adsystem, the substrate, and the gas-phase molecule, respectively. Nudged elastic band (NEB) method and potential energy surface (PES) calculations are performed using a six-layer slab, where the lowest layer is frozen. Here the force threshold is reduced to 0.02 eV/Å as well. This introduces an adsorption energy error bar of less than 0.02 eV. The sampling points of the PES are separated by 0.96 Å in the [100] and [010] directions. At these sampling points, the carbene C atom is fixated laterally. All other degrees of freedom are allowed to relax freely. Four different initial configurations are probed for each sampling point.

Two different adsorption configurations (Figure 2) are probed for each of the three molecular species shown in Figure 1: the carbene insertion into the Si–H bond of a fully H-terminated Si surface[36] (denoted as **I** in the following) and a dative bond to a defect site. In the latter case (denoted as **II**), it is assumed that the molecule bonds to a non-hydrogen saturated Si dimer. Bonding scenarios **I** and **II** differ by the amount of surface-adsorbed hydrogen. In order to compare them energetically, the hydrogen chemical potential μ_H as a function of the surface preparation conditions, i.e., temperature

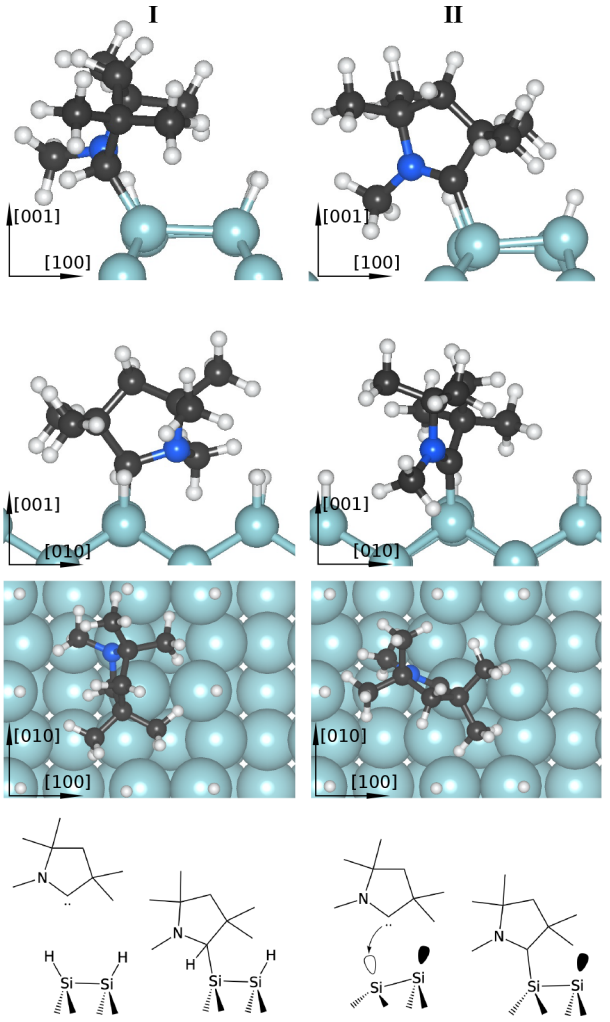

Figure 2. Comparison of the two bonding scenarios for the exemplary case of **1**.

T and partial pressure p, has to be taken into account. This is done here by calculating the thermodynamic potential

$$\Omega \approx U - n_H \mu_H \quad (2)$$

with $U = E_{tot} - E_{s,clean} - E_m$, where $E_{s,clean}$ is the energy of the Si(001) surface without hydrogen termination and n_H refers to the number of hydrogen atoms. The deviation of the hydrogen chemical potential from its molecular energy is approximated by the expression for an ideal two-atom gas,

$$\Delta\mu_H = \frac{kT}{2}\left[\ln\left(\frac{pV_q}{kT}\right) - \ln Z_{rot} - \ln Z_{vib}\right] \quad (3)$$

Here $V_q = (h^2/2\pi mkT)^{3/2}$ is the quantum volume, and Z_{rot} and Z_{vib} are the rotational and vibrational partition functions, respectively.

RESULTS AND DISCUSSION

In order to determine the most stable adsorption geometry for each molecule in configurations **I** and **II**, different starting configurations are probed. In particular, the angle that the CAACs enclose with the [100] direction was varied (Figure 3). Here a step size of 22.5 was used and all non-symmetry-related adsorption configurations were probed, while no variation of the side-group geometries was initiated. This procedure is

https://doi.org/10.1021/acs.jpcc.2c07316
J. Phys. Chem. C 2023, 127, 1973–1980

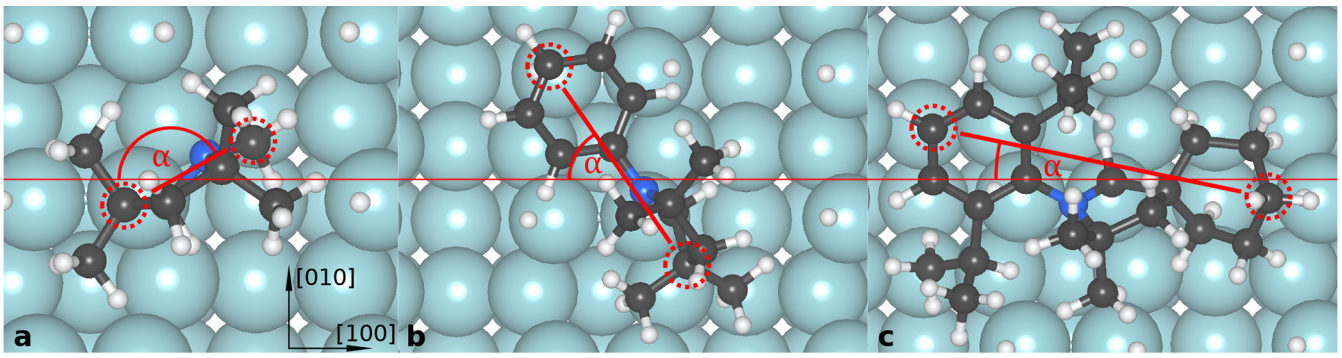

Figure 3. Investigated molecules (a) **1**, (b) **2**, and (c) **3** enclose the angle α with the [100] surface direction.

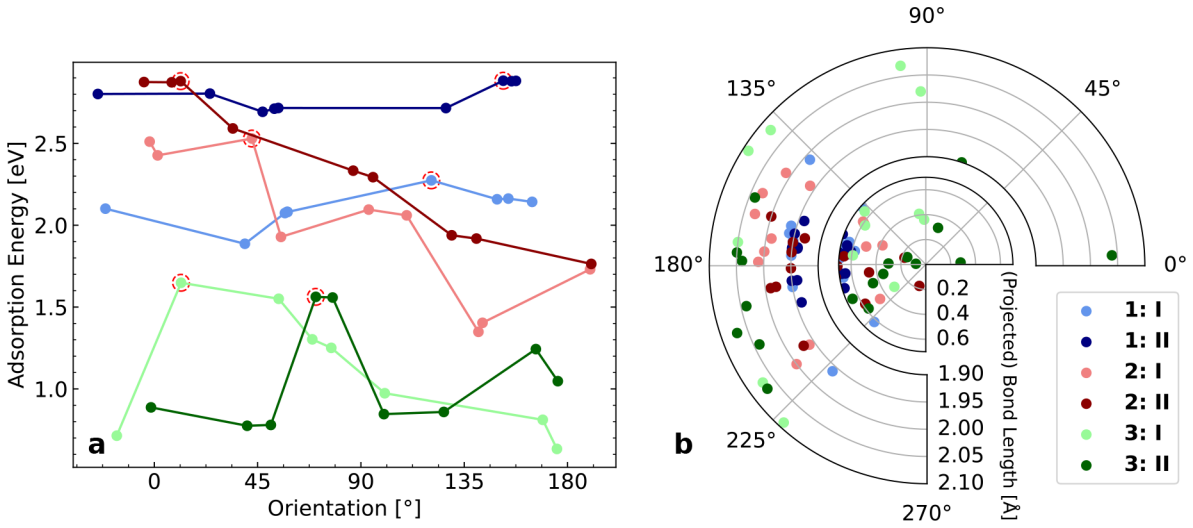

Figure 4. (a) Molecular adsorption energies as a function of molecular orientation. The respective energy maxima are highlighted. (b) Si−C bond lengths and bond orientations relative to the [100] direction. The outer polar chart shows the total bond length d, while the inner chart represents the bond length projected on the (001) plane, $d \sin(\theta)$.

certainly not exhaustive but should provide the most relevant candidates for the subsequent structural relaxation.

The adsorption energy as a function of the molecular orientation is shown in Figure 4a. In the case of **1**, only a small dependence (ΔE_{ads} < 0.4 eV for **I**, ΔE_{ads} < 0.18 eV for **II**) is noted. This can be understood in terms of the small side groups that allow for a nearly free rotation of the molecule. In contrast, a clear dependence of the adsorption energy on the molecular orientation is found for **2**: the highest binding energies are obtained for $\alpha \approx 0°$. In this case, the vdW interaction between the benzene side group with the Si-dimer structure is most favorable. Strong variations of the adsorption energy with several maxima are found in the case of **3**. This results from the large side groups, which sterically interact with the corrugated Si(001):H surface.

In Figure 4b, the variation of the Si−C bond lengths and the azimuth angles between the bond projected on the (001) plane and the [100] direction are shown. Evidently, the CAAC molecules with larger side groups exhibit larger bond lengths (**3**: $d \approx 2.05$ Å) than molecules with small side groups (**1**: $d \approx 1.95$ Å). This is again related to the steric interaction with the substrate. Similar observations were made in ref 8. A majority of azimuth angles range from 135 to 225°, which corresponds to 180 ± 45° and is in line with the orientation expected from the topography of the Si surface.

What determines the adsorption energy in the minimum-energy configurations highlighted with red circles in Figure 4a? In Figure 5, we compare the contributions from van der Waals and chemical bonding as well as molecular and substrate strain to the total adsorption energies of the three CAACs in configurations **I** and **II**. Here the strain contributions to the energy balance are obtained from single-point calculations of

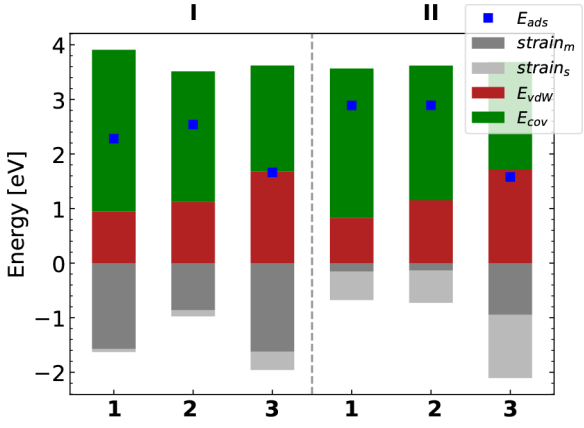

Figure 5. Contributions to the CAAC adsorption energies for the molecular species and adsorption configurations considered here. See the text.

https://doi.org/10.1021/acs.jpcc.2c07316
J. Phys. Chem. C 2023, 127, 1973−1980

the respective systems in both fully relaxed and bonding geometries. For the van der Waals contribution to the energy, we rely on the VASP output. Obviously, **II** results in higher adsorption energies than **I** due to the higher electronegativity of the respective surface bonding sites. As expected, larger molecules experience a stronger vdW attraction to the substrate than smaller ones. At the same time, the larger side groups give rise to a repulsive strain, both in the substrate and in the molecule. The molecular strain is particularly pronounced for configuration **I**, where the H insertion leads to a rehybrization of the carbene C atom from sp^2 to sp^3. Configuration **II**, on the other hand, leads to stronger modifications of the substrate geometry.

However, the energetically most preferable adsorption configuration is determined not only by the adsorption energy but also by the hydrogen chemical potential. This is demonstrated in Figure 6, where we compare the thermodynamic potential changes of the minimum-energy configurations. It can be seen that for hydrogen chemical potentials smaller than −1, −0.8, and −0.6 eV, respectively, dative bonding **II** is more favorable than insertion reaction **I** for **3**, **2**, and **1**. At room temperature and for pressure ranges typical for ultrahigh vacuum, **I** is the stable adsorption configuration for all carbenes investigated. Elevated temperatures are needed to stabilize bonding configuration **II**.

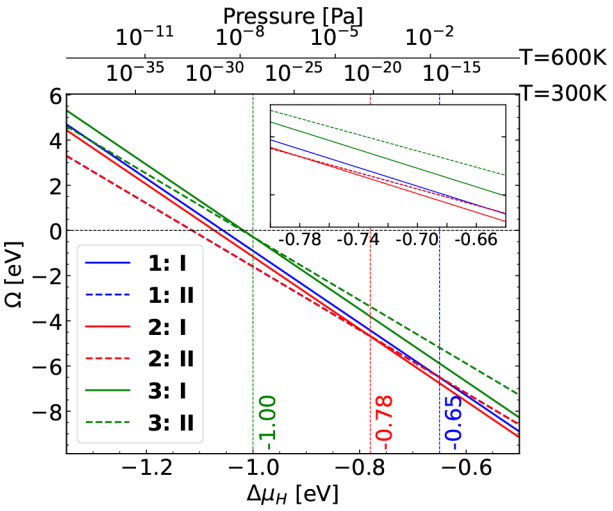

Figure 6. Comparison of the relative stability (in terms of the grand canonical potential) of the CAAC adsorption configurations as a function of the hydrogen chemical potential. The crossing points are indicated. The blue and red dashed lines cannot be discriminated, since the corresponding configurations are nearly degenerate in energy.

Given that the relative stability of **I** and **II** depends on the surface preparation conditions, it is interesting to explore the possibility of transitions between these two bonding configurations. Provided atomic hydrogen is available, **II** will spontaneously transform to **I**. The transition **I** → **II** is studied exemplarily for **3** using the nudged elastic band (NEB) method.[37−39] Starting from the minimum-energy structure of **3** in configuration **I**, at first a hydrogen transfer from the neighboring Si dimer atom to **3** is assumed. This corresponds to step 1 in Figure 7. In step 2, the two hydrogen atoms form H_2 and desorb from the surface. The precise energetics of this process depends again on the hydrogen chemical potential, as indicated in Figure 7. In any event, however, it is an activated process with a minimum-energy barrier of about 0.3 eV.

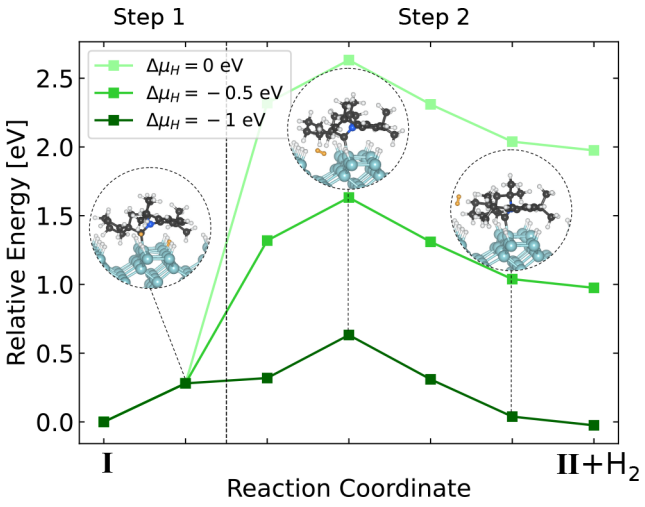

Figure 7. Reaction path for the **I** → **II** transition of **3** including hydrogen desorption. Desorbing H atoms are indicated. The energetics depends on the hydrogen chemical potential, as shown.

The formation of well-ordered molecular overlayers depends on the adsorption/desorption as well as diffusion characteristics of the adsorbed species. This will be investigated next. The NEB calculated reaction paths leading to the adsorption of **1**, **2**, and **3** in configuration **I** are shown in Figure 8. While for **1** and **2** the energy is continuously lowered upon approaching the surface, there exists a precursor state for **3**. An energy barrier of about 0.2 eV needs to be overcome to reach the global minimum-energy structure. The precursor state corresponds to a vdW adsorbed molecule without significant deformations from the gas-phase geometry.

The existence of the precursor state has immediate implications for the potential energy surface experienced by the adsorbed molecules. The respective calculations are shown in Figure 9. In the case of bonding scenario **I**, diffusion barriers of 1.7 and 1.8 eV have been found for **1** and **2**, respectively, regardless of the diffusion direction. In contrast, **3** experiences no significant diffusion barriers as long as it remains solely vdW bound to the surface, i.e., remains in the precursor state *A* shown in Figure 9c. Obviously, suitably chosen side groups allow for tuning the diffusion characteristics.

This holds to some extent even if the attraction to a surface defect site, modeled here as an unsaturated Si dimer, is considered (Figure 9d−f). **1** and **2** are strongly attracted to the surface defect and experience barriers of about 2 eV along [010] and 2.4 eV along [100] between neighboring defect sites. These barriers are significantly reduced to about 1 eV for **3**, as here the reactive carbene atom is sterically protected by the side groups. Generally, the surface defect has a large catchment area, i.e., a large region where the molecules are likely to bond covalently to the substrate. In the case of **1**, the catchment area extends nearly to the whole unit cell. Within the catchment area, further bonding scenarios may occur that affect the structural integrity of the substrate, as shown in Figure 9g.

Finally, the modification of the Si(001):H surface electronic properties due to CAAC adsorption is investigated. In Figure 10, the electronic densities of states for the most stable adsorption geometries are compared with data for clean

https://doi.org/10.1021/acs.jpcc.2c07316
J. Phys. Chem. C 2023, 127, 1973−1980

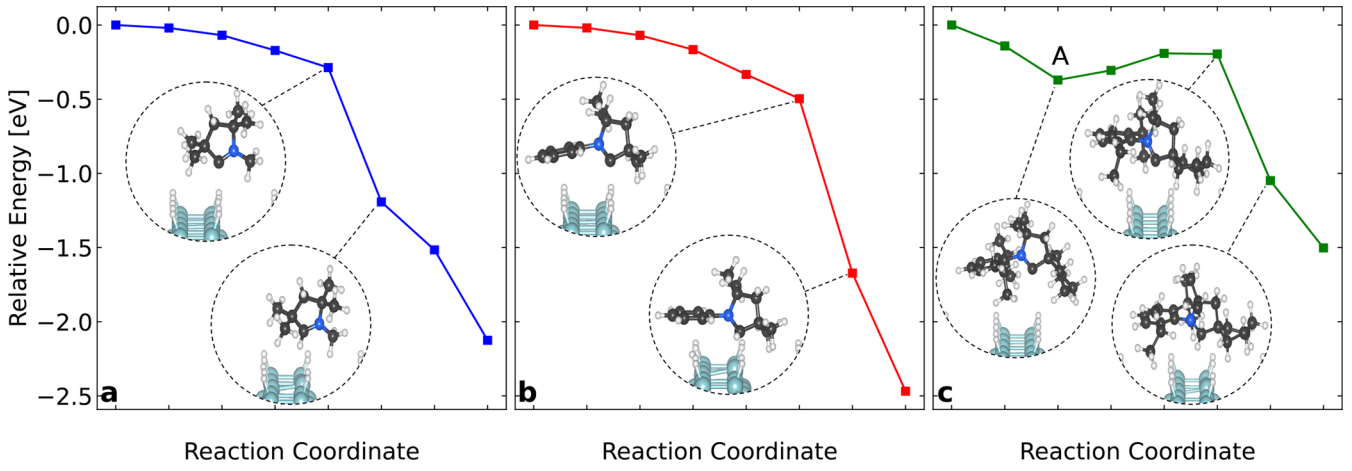

Figure 8. Reaction paths leading to the H insertion of (a) **1**, (b) **2**, and (c) **3**, i.e., the respective configuration **I**. For **3**, an energy barrier of 0.18 eV has to be overcome.

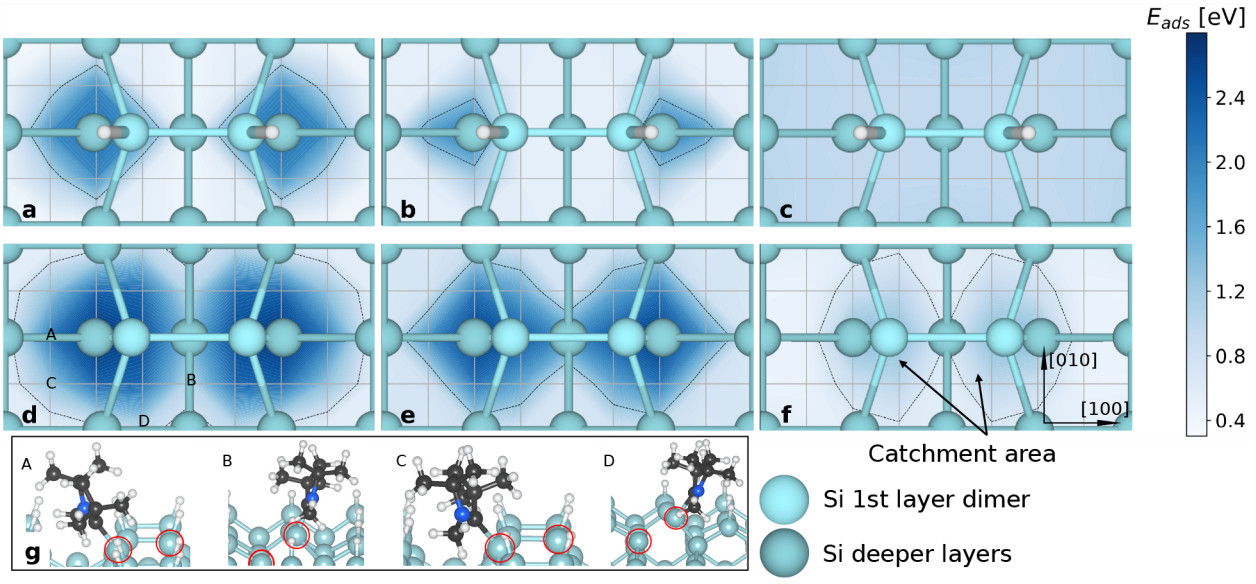

Figure 9. Potential energy surfaces (PES) for bonding scenario **I**, with **1**, **2**, and **3** shown in a−c, respectively. The PESs for the attachment of **1**, **2**, and **3** to an unsaturated Si dimer are shown in d−f, respectively. g shows the adsorption structures resulting from the attachment of **1** to the specific sites indicated in d.

surfaces. The DOS values for the perfect monohydride surface and the surface including an unsaturated Si dimer are shown in Figure 10e,a, respectively. In the latter case, dimer-related surface states P1 and P2 occur close to the Si bulk band edges. P1 is due to an s-like state at the "up" dimer atom. It is energetically lower than the sp^3 hybrid orbitals of bulk Si and occurs below the valence band maximum (VBM).[1] P2 is close to the conduction band minimum (CBM) and corresponds to the unoccupied p-like orbital of the "down" dimer atom.[40−44] The adsorption of CAACs to the surface defect modifies P1 and P2 to P1′ and P2′, respectively; see also Figure 10i, in which the shift P1 → P1′ of the "up" dimer atom state results from the rehybridization of the s-like dangling bond orbital to an sp^3-like dangling bond due to molecular attachment at the "down" dimer atom. The shift P2 → P2′ is due to the transformation of the formerly unoccupied Si surface state at the "down" dimer atom to a dative bond filled with two electrons of the carbene C atom: the dative bond formation results in a low-energy bonding orbital located in the valence band and an antibonding orbital P2′ higher in energy than the formerly unoccupied p orbital P2. The shift P2 → P2′ is largest for **1**, less pronounced for **2**, and hardly visible for **3**. This is due to the different Si−C bond strengths discussed above. In the case of the insertion reaction **I** at the ideal monohydride surface, the adsorption of **1** and **2** gives rise to pronounced peaks M1 and M2 close to the VBM, as shown in Figure 10f,g. They correspond to molecular states (Figure 10i). Obviously, the existence and energetic position of band gap states, often detrimental for applications due to charge carrier recombination, can be tuned by modifying the molecular species.

Similar to earlier observations,[21] CAAC adsorption on Si(001):H is found to reduce the surface work function (Table 1). The work function reduction is particularly strong at the defective Si surface, bonding scenario **II**: in the case of **2** adsorption, a reduction by 1.44 eV is calculated. The work function reduction due to the insertion reaction **I** is less pronounced. It amounts roughly to 0.5 eV and is essentially explained by the molecular dipole (Table 1).

https://doi.org/10.1021/acs.jpcc.2c07316
J. Phys. Chem. C 2023, 127, 1973−1980

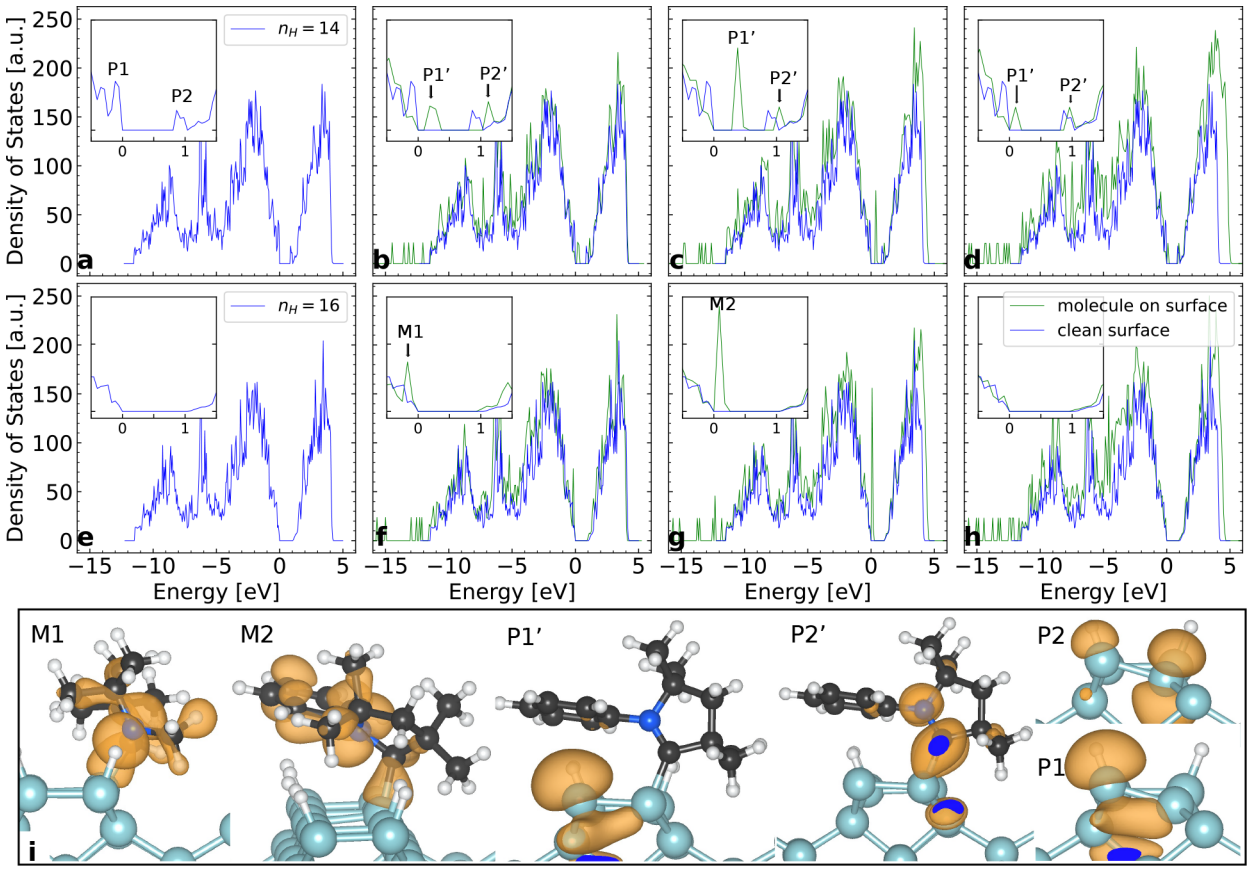

Figure 10. Electronic DOS for **1**, **2**, and **3** adsorption on the surface with an unsaturated Si dimer (b–d) and on the monohydride Si(001):H surface (f–h). The DOS values of the respective surfaces without molecules are shown in a and e, respectively. The energies refer to the valence band maximum at 0 eV. The orbital character of specific peaks is illustrated by isosurfaces in i.

Table 1. Work Function Change of Si(001):H upon CAAC Adsorption[a]

molecule	1		2		3	
bonding scheme	I	II	I	II	I	II
ΔW [eV]	−0.49	−1.16	−0.56	−1.44	−0.55	−1.24
molecular dipole [eV]	−0.43	−0.37	−0.42	−0.48	−0.37	−0.45

[a]The molecular dipole component along the surface normal is given for comparison.

The strong work function reduction of Si upon CAAC adsorption not only will facilitate the electron transport in heterostructures but also can be used to tune the energy barrier at heterojunction interfaces, as well as photoemission, thermoionic emission, absorption, photoluminescence, and catalytic and carrier injection properties of silicon-based electronic devices.

CONCLUSIONS

The energetics, structure, and electronic properties of CAAC adsorbed monohydride Si(001):H surfaces were explored within DFT. The adsorption energy and diffusion characteristics depend largely on the molecular side groups. In particular, it was found that large side groups give rise to a van der Waals bonded precursor state that allows for nearly barrierless diffusion and may assist in the formation of ordered overlayers. While all previous successful attempts to functionalize Si surfaces with ordered NHC overlayers used [111]-oriented substrates and required a boron δ-doping layer underneath the uppermost Si atoms, the present calculations indicate that suitably chosen NHC side groups will allow for the formation of ordered overlayers (i) even in the absence of B doping and (ii) on Si(001) surfaces predominantly used in the micro- and nanoelectronics industry: CAACs weakly attached to the surface by dispersion forces can diffuse at low temperatures to form well-ordered structures. Moderate annealing will then attach the adsorbate to the surface by covalent bond formation.

Surface defects in terms of unsaturated Si dimers act as trapping sites for surface diffusing molecules. The relative stability of dative-bonded and insertion-reacted carbenes depends on the surface preparation conditions and may be varied with the hydrogen partial pressure and temperature. Molecular adsorption on Si(001):H leads to electronic states close to the bulk band edges. These states are more pronounced for strongly bonded small molecules compared to molecules where the reactive carbene atoms are protected by large side groups. CAAC adsorption on silicon strongly reduces its work function. Depending on the bonding scenario and molecular species, reductions by more than 1 eV are calculated.

AUTHOR INFORMATION

Corresponding Author

Wolf Gero Schmidt − *Lehrstuhl für Theoretische Materialphysik, Universität Paderborn, 33095 Paderborn,*

https://doi.org/10.1021/acs.jpcc.2c07316
J. Phys. Chem. C 2023, 127, 1973−1980

Germany; orcid.org/0000-0002-2717-5076;
Email: W.G.Schmidt@upb.de

Author

Lukas Meier − *Lehrstuhl für Theoretische Materialphysik, Universität Paderborn, 33095 Paderborn, Germany*; orcid.org/0000-0001-6185-7532

Complete contact information is available at: https://pubs.acs.org/10.1021/acs.jpcc.2c07316

Notes

The authors declare no competing financial interest.

■ ACKNOWLEDGMENTS

Financial support by the Deutsche Forschungsgemeinschaft (DFG SCHM1361/33) is gratefully acknowledged. We thank the Paderborn Center for Parallel Computing (PC^2) and the Hchstleistungs-Rechenzentrum Stuttgart (HLRS) for grants of high-performance computer time.

■ REFERENCES

(1) Dabrowski, J.; Müssig, H.-J.*Silicon Surfaces and Formation of Interfaces*; World Scientific: Singapore, 2000.
(2) Sze, S.; Li, Y.; Ng, K. K.*Physics of Semiconductor Devices*; Wiley-Interscience: Hoboken, NJ, 2021.
(3) MacQueen, R. W.; Liebhaber, M.; Niederhausen, J.; Mews, M.; Gersmann, C.; Jäckle, S.; Jäger, K.; Tayebjee, M. J. Y.; Schmidt, T. W.; Rech, B.; et al. Crystalline silicon solar cells with tetracene interlayers: the path to silicon-singlet fission heterojunction devices. *Mater. Horiz.* **2018**, *5*, 1065−1075.
(4) Luther, J. M.; Johnson, J. C. An exciting boost for solar cells. *Nature* **2019**, *571*, 38.
(5) Einzinger, M.; Wu, T.; Kompalla, J. F.; Smith, H. L.; Perkinson, C. F.; Nienhaus, L.; Wieghold, S.; Congreve, D. N.; Kahn, A.; Bawendi, M. G.; Baldo, M. A. Sensitization of silicon by singlet exciton fission in tetracene. *Nature* **2019**, *571*, 90−94.
(6) Zhou, Y.; et al. A Universal Method to Produce Low Work Function Electrodes for Organic Electronics. *Science* **2012**, *336*, 327−332.
(7) Weinstein, C. M.; Junor, G. P.; Tolentino, D. R.; Jazzar, R.; Melaimi, M.; Bertrand, G. Highly Ambiphilic Room Temperature Stable Six-Membered Cyclic (Alkyl)(amino)carbenes. *J. Am. Chem. Soc.* **2018**, *140*, 9255−9260.
(8) Zhukhovitskiy, A. V.; Mavros, M. G.; Queeney, K. T.; Wu, T.; Van Voorhis, T.; Johnson, J. A. Reactions of Persistent Carbenes with Hydrogen-Terminated Silicon Surfaces. *J. Am. Chem. Soc.* **2016**, *138*, 8639−8652.
(9) Arduengo, A. J.; Harlow, R. L.; Kline, M. A stable crystalline carbene. *J. Am. Chem. Soc.* **1991**, *113*, 361−363.
(10) Hopkinson, M. N.; Richter, C.; Schedler, M.; Glorius, F. An overview of N-heterocyclic carbenes. *Nature* **2014**, *510*, 485.
(11) Zhukhovitskiy, A. V.; MacLeod, M. J.; Johnson, J. A. Carbene Ligands in Surface Chemistry: From Stabilization of Discrete Elemental Allotropes to Modification of Nanoscale and Bulk Substrates. *Chem. Rev.* **2015**, *115*, 11503−11532.
(12) Crudden, C. M.; et al. Simple direct formation of self-assembled N-heterocyclic carbene monolayers on gold and their application in biosensing. *Nat. Commun.* **2016**, *7*, 12654.
(13) Wang, G.; Rühling, A.; Amirjalayer, S.; Knor, M.; Ernst, J. B.; Richter, C.; Gao, H.-J.; Timmer, A.; Gao, H.-Y.; Doltsinis, N. L.; et al. Ballbot-type motion of N-heterocyclic carbenes on gold surfaces. *Nat. Chem.* **2017**, *9*, 152.
(14) Jiang, L.; Zhang, B.; Médard, G.; Seitsonen, A. P.; Haag, F.; Allegretti, F.; Reichert, J.; Kuster, B.; Barth, J. V.; Papageorgiou, A. C. N-Heterocyclic carbenes on close-packed coinage metal surfaces: bis-carbene metal adatom bonding scheme of monolayer films on Au, Ag and Cu. *Chem. Sci.* **2017**, *8*, 8301−8308.
(15) Bakker, A.; Timmer, A.; Kolodzeiski, E.; Freitag, M.; Gao, H. Y.; Mönig, H.; Amirjalayer, S.; Glorius, F.; Fuchs, H. Elucidating the Binding Modes of N-Heterocyclic Carbenes on a Gold Surface. *J. Am. Chem. Soc.* **2018**, *140*, 11889−11892.
(16) Inayeh, A.; Groome, R. R. K.; Singh, I.; Veinot, A. J.; de Lima, F. C.; Miwa, R. H.; Crudden, C. M.; McLean, A. B. Self-assembly of N-heterocyclic carbenes on Au(111). *Nat. Commun.* **2021**, *12*, 4034.
(17) Krzykawska, A.; Wrobel, M.; Koziel, K.; Cyganik, P. N-Heterocyclic Carbenes for the Self-Assembly of Thin and Highly Insulating Monolayers with High Quality and Stability. *ACS Nano* **2020**, *14*, 6043−6057.
(18) Jain, M.; Gerstmann, U.; Schmidt, W. G.; Aldahhak, H. Adatom mediated adsorption of N-heterocyclic carbenes on Cu(111) and Au(111). *J. Comput. Chem.* **2022**, *43*, 413−420.
(19) Crudden, C. M.; Horton, J. H.; Ebralidze, I. I.; Zenkina, O. V.; McLean, A. B.; Drevniok, B.; She, Z.; Kraatz, H.-B.; Mosey, N. J.; Seki, T.; et al. Ultra stable self-assembled monolayers of N-heterocyclic carbenes on gold. *Nat. Chem.* **2014**, *6*, 409.
(20) Aslanov, L. A.; Zakharov, V. N.; Zakharov, M. A.; Kamyshny, A. L.; Magdassi, S.; Yatsenko, A. V. Stabilization of silicon nanoparticles by carbenes. *Russian Journal of Coordination Chemistry volume* **2010**, *36*, 330.
(21) Franz, M.; et al. Controlled growth of ordered monolayers of N-heterocyclic carbenes on silicon. *Nat. Chem.* **2021**, *13*, 828−835.
(22) Lavallo, V.; Canac, Y.; Präsang, C.; Donnadieu, B.; Bertrand, G. Stable Cyclic (Alkyl)(Amino)Carbenes as Rigid or Flexible, Bulky, Electron-Rich Ligands for Transition-Metal Catalysts: A Quaternary Carbon Atom Makes the Difference. *Angew. Chem., Int. Ed.* **2005**, *44*, 5705−5709.
(23) Soleilhavoup, M.; Bertrand, G. Cyclic (Alkyl)(Amino)Carbenes (CAACs): Stable Carbenes on the Rise. *Acc. Chem. Res.* **2015**, *48*, 256−266.
(24) Bakker, A.; Freitag, M.; Kolodzeiski, E.; Bellotti, P.; Timmer, A.; Ren, J.; Schulze Lammers, B.; Moock, D.; Roesky, H. W.; Mönig, H.; et al. An Electron-Rich Cyclic (Alkyl)(Amino)Carbene on Au(111), Ag(111), and Cu(111) Surfaces. *Angew. Chem., Int. Ed.* **2020**, *59*, 13643−13646.
(25) Kresse, G.; Furthmüller, J. Efficiency of ab-initio total energy calculations for metals and semiconductors using a plane-wave basis set. *Comput. Mater. Sci.* **1996**, *6*, 15−50.
(26) Perdew, J. P.; Burke, K.; Ernzerhof, M. Generalized Gradient Approximation Made Simple. *Phys. Rev. Lett.* **1996**, *77*, 3865−3868.
(27) Ortmann, F.; Schmidt, W. G.; Bechstedt, F. Attracted by Long-Range Electron Correlation: Adenine on Graphite. *Phys. Rev. Lett.* **2005**, *95*, 186101.
(28) Ortmann, F.; Bechstedt, F.; Schmidt, W. G. Semiempirical van der Waals correction to the density functional description of solids and molecular structures. *Phys. Rev. B* **2006**, *73*, 205101.
(29) Grimme, S.; Antony, J.; Ehrlich, S.; Krieg, H. A consistent and accurate ab initio parametrization of density functional dispersion correction (DFT-D) for the 94 elements H-Pu. *J. Chem. Phys.* **2010**, *132*, 154104.
(30) Grimme, S.; Ehrlich, S.; Goerigk, L. Effect of the damping function in dispersion corrected density functional theory. *J. Comput. Chem.* **2011**, *32*, 1456−1465.
(31) Blöchl, P. E. Projector augmented-wave method. *Phys. Rev. B* **1994**, *50*, 17953−17979.
(32) Kresse, G.; Joubert, D. From ultrasoft pseudopotentials to the projector augmented-wave method. *Phys. Rev. B* **1999**, *59*, 1758−1775.
(33) Northrup, J. E. Structure of Si(100)H: Dependence on the H chemical potential. *Phys. Rev. B* **1991**, *44*, 1419−1422.
(34) Monkhorst, H. J.; Pack, J. D. Special points for Brillouin-zone integrations. *Phys. Rev. B* **1976**, *13*, 5188−5192.
(35) Blöchl, P. E.; Jepsen, O.; Andersen, O. K. Improved tetrahedron method for Brillouin-zone integrations. *Phys. Rev. B* **1994**, *49*, 16223−16233.
(36) Doyle, M. P.; Duffy, R.; Ratnikov, M.; Zhou, L. Catalytic Carbene Insertion into C-H Bonds. *Chem. Rev.* **2010**, *110*, 704−724.

(37) Jónsson, H.; Mills, G.; Jacobsen, K.*Classical and Quantum Dynamics in Condensed Phase Simulations*; World Scientific, 1998.
(38) Henkelman, G.; Uberuaga, B.; Jónsson, H. A climbing image nudged elastic band method for finding saddle points and minimum energy paths. *J. Chem. Phys.* **2000**, *113*, 9901−9904.
(39) Henkelman, G.; Jónsson, H. Improved tangent estimate in the nudged elastic band method for finding minimum energy paths and saddle points. *J. Chem. Phys.* **2000**, *113*, 9978−9985.
(40) Chadi, D. J. Atomic and Electronic Structures of Reconstructed Si(100) Surfaces. *Phys. Rev. Lett.* **1979**, *43*, 43−47.
(41) Yin, M. T.; Cohen, M. L. Theoretical determination of surface atomic geometry: Si(001)-(2 × 1). *Phys. Rev. B* **1981**, *24*, 2303−2306.
(42) Hamers, R.; Tromp, R.; Demuth, J. Electronic and geometric structure of Si(111)-(7 × 7) and Si(001) surfaces. *Surf. Sci.* **1987**, *181*, 346−355.
(43) Dabrowski, J.; Scheffler, M. Self-consistent study of the electronic and structural properties of the clean Si (001)(2 × 1) surface. *Appl. Surf. Sci.* **1992**, *56*, 15−19.
(44) Ramstad, A.; Brocks, G.; Kelly, P. J. Theoretical study of the Si(100) surface reconstruction. *Phys. Rev. B* **1995**, *51*, 14504−14523.

https://doi.org/10.1021/acs.jpcc.2c07316
J. Phys. Chem. C 2023, 127, 1973−1980